Outer radiation belt dropout dynamics following the arrival of two interplanetary coronal mass ejections

Alves, L. R.,[1] L. A. Da Silva,[1] V. M. Souza,[1] D. G. Sibeck,[2] P. R. Jauer,[1] L. E. A. Vieira,[1] B. M. Walsh,[3] M. V. D. Silveira,[2] J. P. Marchezi,[1] M. Rockenbach,[1] A. Dal Lago,[1] O. Mendes,[1] B. T. Tsurutani,[4] D. Koga,[1] S. G. Kanekal,[2] D. N. Baker,[5] J. R. Wygant,[6] C. A. Kletzing[7]

Magnetopause shadowing and wave-particle interactions are recognized as the two primary mechanisms for losses of electrons from the outer radiation belt. We investigate these mechanisms, using satellite observations both in interplanetary space and within the magnetosphere and particle drift modeling. Two interplanetary shocks/sheaths impinged upon the magnetopause causing a relativistic electron flux dropout. The magnetic cloud (MC) and interplanetary structure sunward of the MC had primarily northward magnetic field, perhaps leading to a concomitant lack of substorm activity and a ten day-long quiescent period. The arrival of two shocks caused an unusual electron flux dropout. Test-particle simulations have shown $\sim$ 2 to 5 MeV energy, equatorially mirroring electrons with initial values of $L \geq 5.5$ can be lost to the magnetosheath via magnetopause shadowing alone. For electron losses at lower L-shells, coherent chorus wave-driven pitch angle scattering and ULF wave-driven radial transport have been shown to be viable mechanisms.

[1]Instituto Nacional de Pesquisas Espaciais/INPE, São José dos Campos, São Paulo, Brasil.

[2]NASA Goddard Space Flight Center, Greenbelt, Maryland, USA.

[3]Space Sciences Laboratory, University of California, Berkeley, California, USA.

[4]Jet Propulsion Laboratory, California Institute of Technology, Pasadena, California, USA.

[5]Laboratory for Atmospheric and Space Physics, University of Colorado, Boulder, Colorado, USA.

[6]School of Physics and Astronomy, University of Minnesota, Minneapolis, Minnesota, USA.

[7]Department of Physics and Astronomy, University of Iowa, Iowa City, Iowa, USA.

1. Introduction

The relativistic electron population trapped in the outer radiation belt in the Earth's magnetosphere is known to be highly dynamic [*Reeves et al.*, 2003; *Turner et al.*, 2013]. The particles are known be accelerated and to be lost by various competing mechanisms operating in time scales from a few seconds to several days [*Green and Kivelson*, 2004; *Horne et al.*, 2005; *Miyoshi and Kataoka*, 2005; *Borovsky and Denton*, 2006; *Bortnik et al.*, 2006; *Su et al.*, 2010, 2011a, b; *Reeves et al.*, 2013; *Turner et al.*, 2014a; *Hajra et al.*, 2015]. *Kilpua et al.* [2015] showed that the radiation belt response is organized according to the large-scale solar wind driver structure and the sequence at which they arrive. In particular sheaths and coronal mass ejection (CME) can lead to the deep and long radiation belt depletion (see also *Hietala et al.* [2014]). Our interest in this paper is the loss process.

There are some well known loss processes, including "magnetopause shadowing" where particles gradient drift in an overcompressed dayside magnetosphere into the magnetopause and are lost to the magnetosheath [*Keika et al.*, 2005; *Matsumura et al.*, 2011; *Glauert et al.*, 2014]. The particle's motion to outer L-shells can be caused by adiabatic and nonadiabatic transport mechanisms [*Shprits et al.*, 2006; *Su et al.*, 2010, 2011a]. Also, cyclotron resonant wave particle interactions cause particles to be pitch angle scattered into the loss cone and lost into the ionosphere (e.g. [*Shprits et al.*, 2008]). For the latter mechanism, there are two possible wave modes that have been mentioned as being important: electromagnetic whistler mode chorus which is generated by the 10-100 keV electron temperature anisotropy [*Tsurutani and Smith*, 1974, 1977; *Shprits et al.*, 2007, 2008; *Lakhina et al.*, 2010; *Lam et al.*, 2010; *Tsurutani et al.*, 2013] and electromagnetic ion cyclotron (EMIC) waves which are generated by the 10-100 keV proton temperature anisotropy [*Thorne and Kennel*, 1971; *Lyons and Thorne*, 1972; *Thorne*, 2010; *Turner et al.*, 2014a]. For the latter interaction, the relativistic electrons overtake the waves or are in "anomalous cyclotron resonance" [*Tsurutani and Lakhina*, 1997].

On late September 11, 2014 an interplanetary coronal mass ejection (ICME) hit the Earth's magnetosphere. Around 17 hours later a second shock reached the Earth. Following these two events, an unusual relativistic outer belt electron flux dropout was observed by multiple spacecraft at different local times wherein the fluxes fell ~ 1 order of magnitude below their previous undisturbed levels. Such a scenario lasted for at least 10 days.

Section 2 describes the electron flux dropout event. Section 3 is devoted to an investigation of the possible loss mechanisms previously invoked to explain observed electron flux decreases occurring at $L^* \gtrsim 4$ such as coherent chorus wave-driven pitch angle scattering (Section 3.1), magnetopause shadowing (Section 3.2), and adiabatic and nonadiabatic radial transport (Section 3.3). Although EMIC waves can interact efficiently with relativistic electrons, leading to rapid flux dropouts during storm-time periods [Ukhorskiy et al., 2010; Su et al., 2011b, 2012], in this event there was no spacecraft coverage on the dusk side to identify EMIC waves. Thus, the contribution of EMIC waves is out of the scope of this work. Nevertheless, the Van Allen Probe A data covered the dawn side of the magnetosphere where they could detect whistler mode chorus waves. Lastly, the summary and discussion are presented in Section 4.

2. Electron Flux Dropout after the Arrival of two Interplanetary Shocks

Data from the Magnetometer (MAG) [*Smith et al.*, 1998] and Solar Wind Electron, Proton, and Alpha Monitor (SWEPAM) [*McComas et al.*, 1998] instruments onboard the Advanced Composition Explorer (ACE) satellite are used to identify the magnetic field and plasma characteristics of both September 11 and 12, 2014 interplanetary shocks/sheaths which are associated with the relativistic electron flux dropout event reported in this work. The shocks are characterized, respectively, by magnetosonic mach numbers (M_{ms}) of $\sim$ 2.0 and $\sim$ 2.4, [*Paschmann and Daly*, 1998]. They were detected by the ACE satellite at 22:57:58 UT on September 11 and, at 15:22:42 UT on September 12, respectively, as indicated by the two vertical solid lines in Figure 1.

The shock structures are evidenced by the sharp and simultaneous changes in solar wind speed (Figure 1c), dynamic pressure (d), and interplanetary magnetic field (IMF) intensity, B_t, and north-south B_z component (e). Following the arrival of these interplanetary structures, the outer radiation belt ($4.0 \lesssim L^* \lesssim 5.5$) electron flux underwent an approximately 1 order of magnitude decrease at the 1.8–4.5 MeV energy range as measured by the Relativistic Electron Proton Telescope (REPT) [*Baker et al.*, 2013] instrument onboard the Van Allen Probes A and B. Figure 1 (a) shows REPT's A 1.8 MeV energy channel electron flux as a function of time and the L^* parameter [*Roederer*, 1970] which is related to the third adiabatic invariant. Right after the first shock ($M_{ms} \sim 2.0$) arrival, the flux decreased primarily in the outskirts of the outer belt, i.e., at $L^* \gtrsim 5$ (horizontal continuous line), in around 12 hours. For this case, the post-shock IMF Bz component was fluctuating about a mean value near zero ($B_z^{average} \sim 0.3$ nT), and reached negative values as large as -14 nT. Large auroral activity (AE > 500 nT) was present during that time, although no major ring current response occurred (SYM-H > -25 nT). The second (and stronger) shock ($M_{ms} \sim 2.4$) reached the magnetosphere approximately 17 hours later, causing a further decrease in electron fluxes within the same energy channels mentioned above, but this time for the entire outer belt (Figure 1 (b)). This decrease took place when both auroral and ring current activities were enhanced, i.e., AE > 500 nT and minimum SYM-H $= -75$ nT, respectively, which coincided with the period when the sheath's Bz component was oscillating between positive and negative values. The magnetic cloud (MC) that followed the second shock and the interplanetary structure sunward of the MC had a $\sim$ 3 day-long positive IMF Bz component and thus no significant auroral activity occurred during that time. This observation agrees with previous work [*Tsurutani and Gonzalez*, 1995; *Du et al.*, 2008] which has shown that auroral activity is needed for the radiation belt repopulation. Meanwhile, the entire outer radiation belt remained in a quiescent state where fluxes remained low and practically no sign of repopulation was detected by the REPT's instrument for a period of ten days. This unusual relativistic electron flux dropout with no concurrent repopulation nicely separated loss and acceleration processes for relativistic electrons.

The electron flux dropout which occurred after the second interplanetary shock arrival was also observed at different local times (LT) and energies. The Solid State Telescopes (SST) onboard the THEMIS A, D, and E [*Angelopoulos*, 2008] spacecraft (Figure S1) measured a nearly one order of magnitude decrease in the electron flux at $L \sim 5$ for the $\sim$ 719 keV energy channel around 22:30 LT. At geosynchronous orbit the high-energy (0.6 -

2 MeV) electron flux decreased also by roughly one order of magnitude as observed near 12 LT by the Energetic Particle Sensor (EPS) onboard the GOES 13 satellite (not shown).

3. Loss Mechanisms for $L^* \gtrsim 4$

3.1. Whistler Mode Chorus Waves Contribution

Discrete whistler mode chorus waves were excited within the outer radiation belt ($3 \lesssim L^* \lesssim 7$), and detected by the Van Allen Probe A in the dawn side sector (05–07 Magnetic Local Time, MLT) on September 12 (Figure S2). We investigate analytically [*Kennel and Petschek*, 1966] at 05:00 MLT, and $L^* \sim 5$, whether observed chorus waves amplitudes were high enough to pitch angle-scatter those electrons into the loss cone, after the second interplanetary shock arrival (vertical dashed line in Figure S2).

We concentrate our analysis by looking at the 21:25 – 22:00 UT interval (gray shaded area in Figure S2) for two reasons: 1) the spacecraft was within 2 degrees of the magnetic equator where chorus waves are expected to be generated [*Tsurutani and Smith*, 1974, 1977; *Omura et al.*, 2008] and therefore they can be assumed to be coherent, and 2) high intensity magnetic spectral density related to chorus waves was detected (Figure 2a). Additionally, EMFISIS [*Kletzing et al.*, 2013] magnetic field data acquired in burst mode ($\sim$10–12.000 Hz) were available for some short intervals in this period (black and red arrows in Figure 2a).

For our calculation, we considered the interaction of relativistic, parallel (to the equatorial ambient magnetic field vector $\mathbf{B}_o$) propagating electrons with several chorus subelements [*Tsurutani et al.*, 2009; *Santolík et al.*, 2014] as shown in Figure 2 (b). For each subelement, we compute the change in pitch angle ($\Delta\alpha$) undergone by an equatorially mirroring (90° pitch angle) electron as a result of the cyclotron resonant interaction for two different cases: for the first one we consider the electron to be in resonance with the chorus wave for the whole subelement period (τ), but the second one for only one wave cycle period (T) (see Figure 2b). In this way, we estimate $\Delta\alpha$ [*Kennel and Petschek*, 1966] for both longer ($\Delta\alpha_\tau$) and shorter ($\Delta\alpha_T$) times of interaction, since one cannot know in advance for how much time the particle is going to be in resonance with the wave.

$$\Delta\alpha_i = \frac{B_{max}}{B_o}\frac{\Omega}{\gamma}\Delta t_i. \tag{1}$$

In equation 1, B_{max} and B_o are, respectively, the peak instantaneous wave packet amplitude and the equatorial ambient magnetic field magnitude, Ω the electron cyclotron frequency, γ the Lorentz factor, and $\Delta t_i = iV_g/V_s$ the estimated interaction time [*Lakhina et al.*, 2010], where i can be either τ or T. The term Δt_i is the ratio between the chorus subelement's scale size iV_g, where V_g is the group velocity, and the relativistic relative velocity V_s between the chorus wave and the electron's parallel resonant velocity calculated in the satellite frame.

Table 1 shows the parameters obtained from direct data observation namely, τ, T, B_{max}, B_o, and f (chorus subelement frequency, $f \approx 1/T$) and the derived parameters Ω, Δt_τ, Δt_T, $\Delta\alpha_\tau$, $\Delta\alpha_T$, for the chosen time interval, 21:25–22:00 UT. The majority of chorus subelements had a duration τ corresponding to 3.0 to 4.5 wave cycles T (see Figure 2 b), i.e., $\tau \sim 4T$. Only for one case (subelement 9) we had $\tau \sim 6 - 7T$.

On the one hand, considering the longer interaction times between the electron and chorus subelements, i.e., larger than three wave cycle periods, the estimated change in pitch angle $\Delta\alpha_\tau$ was within $\sim 3.0^\circ$ and $\sim 10.3^\circ$. On the other hand, for shorter interaction times $\Delta\alpha_T$ was considerably lower with values ranging from $\sim 0.8^\circ$ up to 1.5°. Thus, for the analysed case of ∼2.0 MeV relativistic electrons interacting with coherent chorus waves observed during 21:25–22:00 UT on September 12, the pitch angle scattering contribution for the outer belt electron loss can be relevant only in the limit where the resonant interaction exceeds at least three wave cycle periods. For higher electron energies, our calculation shows a decrease in $\Delta\alpha$, which indicates the cyclotron resonant interaction is less effective as the electron energy increases.

3.2. Test-particle Magnetopause Shadowing Modeling

We investigate whether magnetopause shadowing alone would be sufficient to deplete the entire outer radiation belt. Thus, a test-particle approach is employed in order to follow the azimuthal drift orbit of a single equatorially mirroring (90° pitch angle) electron during the time when the magnetosphere was most compressed due to the arrival of the second interplanetary shock on September 12, 2014. Looking at ACE's time-lagged plasma data, the solar wind dynamic pressure was the highest (∼14 nPa), around 17:00 UT on September 12. We have run the global MHD Block-Adaptive Tree Solarwind Roe Upwind Scheme (BATS-R-US) code [*Tóth et al.*, 2011] coupled to the Comprehensive Ring Current Model (CRCM) [*Glocer et al.*, 2013] in a steady-state mode for the perturbed period to obtain a realistic configuration for the near-Earth magnetic environment. In particular, the IMF value used for running the code was (B_X, B_Y, B_Z) = (-9.63,13.48,11.20) nT. The next step was to integrate the relativistic Lorentz equation

$$\frac{d\mathbf{V}}{dt} = -\frac{e}{\gamma m_e}\mathbf{V} \times \mathbf{B}, \tag{2}$$

for an electron with an equatorial pitch angle of 90° using the magnetic field vector $\mathbf{B}$ modeled by BATS-R-US. In equation 2, $\gamma = 1 + E/m_e c^2$ is the Lorentz factor, E is the electron initial energy, m_e the electron rest mass, -e the electron charge, c the speed of light, and $\mathbf{V}$ the electron velocity. For the electron initial energy E, we used both 1.8 and 4.5 MeV values corresponding to the energy range at which the electron flux dropout was observed by the REPT's instrument. Lastly, equation 2 is solved by means of a fifth-order Runge-Kutta method.

We test the consequence of different initial locations in the integration of the electron azimuthal drift orbit. Electron orbits are set to start at distinct points in the Geocentric Solar Magnetospheric (GSM) equatorial plane, i.e. (Y,Z) = (0,0), with the following X coordinates: -8, -7, -6.6, -6, -5.5, -5 and -4.5 R_E. In all cases the electron initially drifts towards the dawn side magnetosphere, as expected. For orbits starting at distances greater than or equal to geosynchronous orbit ($X \leq -6.6\,R_E$, Figure 3a) the electron does not complete a full azimuthal orbit. Instead, a sharp change in its orbit occurs when it reaches the modeled BATS-R-US magnetopause in the 06–09 local time sector: its guiding center moves towards increasingly negative values of the Z_{GSM} coordinate while the particle continues its drifting path towards the noon-meridian. Upon reaching the southern cusp the electron escapes to the magnetosheath region (Figure 3a). Thus, the outermost part of the outer belt, i.e. at or beyond geosynchronous orbit, could have their electrons lost to the magnetosheath by magnetopause shadowing. For orbits with radial distances starting inside geosynchronous (X = -6 R_E, Figure 3b), the electron does complete a full azimuthal orbit, but it is lost to the magnetosheath in the second one. Initially, as the electron approaches the modeled dayside magnetopause, its original bouncing path is distorted, i.e. its mirror points are increased from Z $\sim \pm 0.8\,R_E$ at the nightside sector up to Z $\sim \pm 2\,R_E$ at the dayside sector. Such a distortion is further enhanced during the following (second) orbit causing the loss of the electron to the magnetosheath (Figure 3b). We note that for energies higher than 2.0 MeV (and lower than or equal to 4.5 MeV), the electrons are also lost for orbits starting at $L \geq 5.5$. Our simulations showed that electrons located deeper ($L < 5.5$) in the outer radiation belt, however, are not lost to the magnetosheath region due to magnetopause shadowing alone (Figure 3c). Hence, concurrent mechanisms are required to accomplish the observed loss of relativistic electrons deeper inside the outer belt.

3.3. Outward Radial Diffusion and Adiabatic Transport Contributions

According to numerical simulations carried out by *Su et al.* [2010], for $L^* \gtrsim 5$, the observed equatorially mirroring relativistic electron loss (Figure 1b) can be primarily caused by the combined effect of fully adiabatic transport and radial (nonadiabatic) diffusion during the main phase period, i.e., when the SYM-H is decreasing towards its minimum value (-75 nT). In their simulations the latter mechanism which is caused by ULF wave-particle interactions played a minor role. However, for this same period ground magnetometer data (not shown) from the 16–19 LT sector, which differs from that covered by Van Allen Probe A (05–06 LT) indicate the presence of increased ULF waves activity after the first and second interplanetary shock arrivals. We discuss possible causes for electron losses deep inside the outer radiation belt related to these observations. According to a model-data comparison carried out by *Shprits et al.* [2006] outward radial diffusion may explain nonadiabatic electron flux dropouts down to $L^* \sim 4$ during storm-time conditions. In fact, from Figure 1 (b) and Figure S3 one can see that the electron flux decrease at $L^* \sim 4$ is observed along with enhanced global ULF wave activity which in turn is associated with outward radial diffusion. Thus, for the observed electron losses at $L^* \sim 4$ we interpret that both outward radial diffusion and adiabatic transport may lead to relativistic electron flux dropout possibly due to magnetopause losses [*Loto'aniu et al.*, 2010].

4. Summary and Discussion

The relativistic ($1 \lesssim E \lesssim 4.5$ MeV) outer radiation belt electron flux dropout event observed here occurred in $\lesssim 12$ hours following the arrival of two interplanetary shocks with distinct shock strengths, $M_{ms} \sim 2.0$ and 2.4. Data from multipoint observations showed a large scale electron flux decrease from $\sim$ 22:00 – 12:00 LT which lasted for around 10 days.

The relativistic outer belt electron flux dropout observed during the storms main phase is understood as the result of several physical processes occurring simultaneously. Besides, different mechanisms may cause electron flux dropout in different L-shells [*Bortnik et al.*, 2006; *Turner et al.*, 2014b, and references therein]. Among them, resonant wave-driven scattering has been claimed to cause electron losses deep into the magnetosphere (L$\lesssim$ 5); whilst for higher L-shells (L > 5), nonadiabatic and adiabatic radial transport have been proposed to transport electrons to the compressed dayside magnetosphere where they were lost.

For the relativistic electron flux deep in the magnetosphere, the interaction with whistler mode chorus waves result in two concurrent processes namely energy diffusion, i.e., electrons are locally accelerated, and pitch angle scattering to the loss cone. Some recent works using different models have found that wave-particle interaction via chorus waves can be an efficient mechanism for local electron acceleration [*Summers et al.*, 2004; *Li et al.*, 2007; *Thorne*, 2013], even during non storm-time period [*Su et al.*, 2014]. Besides, coherent chorus waves may also be associated to rapid loss in low L-shells [*Horne and Thorne*, 2003; *Thorne et al.*, 2005; *Summers et al.*, 2007, and references therein].

Coherent whistler mode chorus wave activity was enhanced right after the second interplanetary shock arrival, which corresponds to the time interval when Van Allen Probes travel from dawn to noon, i.e. from 5 to 8 MLT. For this period, we estimate analytically the pitch angle scattering of relativistic, equatorially mirroring electrons due to the cyclotron resonant interaction with these waves. We have shown that a pitch angle change in the range of $3\,^{\circ}$–$10\,^{\circ}$ can be achieved when the interaction time exceeds at least three wave cycle periods. This result indicates that wave-particle interaction via coherent chorus waves could have played an important role in the relativistic electron loss observed in this dropout event, despite pitch angle scattering being effective only for those relativistic electrons which are in the vicinity of the loss cone.

The interaction between whistler mode chorus wave and relativistic electrons results in a competition between local acceleration and loss of relativistic electrons into the loss cone [*Horne et al.*, 2003; *Summers et al.*, 2004; *Li et al.*, 2007; *Bortnik and Thorne*, 2007; *Shprits et al.*, 2008]. In particular, the coherent chorus wave-driven pitch angle scattering can be effective when waves are observed to interact with relativistic electrons on the dayside [*Shprits et al.*, 2008]. For relativistic electron's energy below 3 MeV, the acceleration rate is not favoured in regions of high ω_{pe}/Ω_e, i.e. ≥ 5 [*Horne et al.*, 2003] which is true for the present analyzed case where $\omega_{pe}/\Omega_e \geq 6$. Furthermore, chorus wave activity intensified between 5 to 8 MLT, i.e. from dawn side magnetosphere toward the noon region. In such a region chorus wave-driven pitch angle scattering of relativistic electrons is expected to be effective [*Shprits et al.*, 2008]. Thus, our results are in accordance with *Shprits et al.* [2008] and *Horne et al.* [2003], and show an example of the wave-particle interaction which resulted in a net loss of outer belt electrons. We note that EMIC waves may have contributed to the electron depletion at local times other than those covered in this study.

The successive arrival of two interplanetary shocks left different consequences to the outer radiation belt. Following the arrival of the first shock, we verified a dropout mostly restricted to $L^* \geq 5$. The outer belt had not recovered yet when a second and stronger shock hit the Earth's magnetosphere and a second dropout reached the heart of the radiation belt, i.e., $L^* \sim 4$. This scenario is consistent with magnetopause shadowing playing a minor (major) role at the time of the first (second) shock [*Turner et al.*, 2014a, b]. Our test-particle simulations in a compressed, time-stationary magnetic field simulated by the 3D MHD BATS-R-US code showed magnetopause shadowing alone as a plausible loss mechanism for electrons located at or above $L = 5.5$. Below that limit, other mechanisms would be required. We note that our simulations did not include ULF waves, which have shown to play an important role in outer belt electron precipitation [*Brito et al.*, 2015].

According to *Shprits et al.* [2006] nonadiabatic radial transport driven by ULF waves, and adiabatic radial transport can account for the rapid loss of particles from locations that lie deep in the magnetosphere, i.e. from drift paths that do not intersect the magnetopause [*Morley et al.*, 2010a, b; *Bortnik et al.*, 2006]. In this event, such a possibility is reinforced by data observation which showed the electron flux dropout subsided on September 13, roughly at the same time when ULF wave activity was strongly suppressed (see Figure S3).

During the three days following the second shock arrival, i.e., from September 13 up to 16, no substorm activity as probed by the AE index was observed, due to the persistent northward IMF Bz component of both the MC and the interplanetary structure sunward of the MC. During this period, the outer radiation belt was quiet with no sign of relativistic electron repopulation, and chorus wave activity was also strongly suppressed (Figure S4).

Acknowledgments. We would like to thank the Center for Space Environment Modeling (CSEM) at the University of Michigan for providing the numerical SWMF Code available at `http://csem.engin.umich.edu/tools/swmf/downloads.php`. We are also in debt to the NOAA's GOES, THEMIS and Van Allen Probes missions teams; NASA's CDAWeb, TDAS, OMNI and NGDC for online data access and data analysis tools. Solar wind parameters presented in Sections 2 and 3 measured by the ACE satellite are available at `http://www.srl.caltech.edu/ACE/ASC/DATA/browse-data/browse-curr/`. The Van Allen Probes' and THEMIS' missions datasets presented in Section 3 and Supplementary Material are available at CDAWeb `http://cdaweb.gsfc.`

nasa.gov/istp_public/. The SPEDAS code for THEMIS data analysis is available at http://themis.ssl.berkeley.edu/index.shtml.

References

Angelopoulos, V. (2008), The THEMIS mission, *Space Science Reviews*, *141*(1–4), 5–34, doi:10.1007/s11214-008-9336-1.

Baker, D., S. Kanekal, V. Hoxie, S. Batiste, M. Bolton, X. Li, S. Elkington, S. Monk, R. Reukauf, S. Steg, J. Westfall, C. Belting, B. Bolton, D. Braun, B. Cervelli, K. Hubbell, M. Kien, S. Knappmiller, S. Wade, B. Lamprecht, K. Stevens, J. Wallace, A. Yehle, H. Spence, and R. Friedel (2013), The relativistic electron-proton telescope (rept) instrument on board the radiation belt storm probes (rbsp) spacecraft: Characterization of earth's radiation belt high-energy particle populations, in *The Van Allen Probes Mission*, edited by N. Fox and J. Burch, pp. 337–381, Springer US, doi: 10.1007/978-1-4899-7433-4_11.

Borovsky, J. E., and M. H. Denton (2006), Differences between cme-driven storms and cir-driven storms, *Journal of Geophysical Research: Space Physics*, *111*(A7), n/a–n/a, doi:10.1029/2005JA011447, a07S08.

Bortnik, J., and R. M. Thorne (2007), The dual role of ELF/VLF chorus waves in the acceleration and precipitation of radiantion belt electrons, *Journal of Atmospheric and Solar-Terrestrial Pysics*, *69*(3), 378–386, doi:10.1016/j.jastp.2006.05.030.

Bortnik, J., R. M. Thorne, T. P. OBrien, J. C. Green, R. J. Strangeway, Y. Y. Shprits and D. N. Baker(2006), Observation of two distinct, rapid loss mechanism during the 20 November 2003, *Journal of Geophysical Research: Space Physics*, *111*(A12), n/a–n/a, doi:10.1029/2006JA011802.

Brito, T., M. K. Hudson, B. Kress, J. Paral, A. Halford, R. Millan, and M. Usanova (2015), Simulation of ulf wave-modulated radiation belt electron precipitation during the 17 march 2013 storm, *Journal of Geophysical Research: Space Physics*, pp. n/a–n/a, doi:10.1002/2014JA020838.

Du, A. M., B. T. Tsurutani, and W. Sun (2008), Anomalous geomagnetic storm of 21–22 january 2005: A storm main phase during northward imfs, *Journal of Geophysical Research: Space Physics*, *113*(A10), n/a–n/a, doi:10.1029/2008JA013284, a10214.

Glauert, S. A., R. B. Horne, and N. P. Meredith (2014), Simulating the earth's radiation belts: Internal acceleration and continuous losses to the magnetopause, *Journal of Geophysical Research: Space Physics*, *119*(9), 7444–7463, doi:10.1002/2014JA020092.

Glocer, A., M. Fok, X. Meng, G. Toth, N. Buzulukova, S. Chen, and K. Lin (2013), CRCM + BATS–R–US two–way coupling, *Journal of Geophysical Research: Space Physics*, *118*(4), 1635–1650, doi:10.1002/jgra.50221.

Green, J. C., and M. G. Kivelson (2004), Relativistic electrons in the outer radiation belt: Differentiating between acceleration mechanisms, *Journal of Geophysical Research: Space Physics*, *109*(A3), n/a–n/a, doi:10.1029/2003JA010153, a03213.

Hajra, R., B. T. Tsurutani, E. Echer, W. D. Gonzalez, and O. Santolik (2015), Relativistic ($E > 0.6$, > 2.0, and > 4.0 MeV) electron acceleration at geosynchronous orbit during high-intensity, long-duration, continuous ae activity (hildcaa) events, *The Astrophysical Journal*, *799*(1), 39.

Hietala, H., E. K. J. Kilpua, D. L. Turner, and V. Angelopoulos (2014), Depleting effects of icme-driven sheath regions on the outer electron radiation belt, *Geophysical Research Letters*, *41* (7), 2258–2265, doi:10.1002/2014GL059551.

Horne, R. B., R. M. Thorne, S. A. Glauert, J. M. Albert, N. P. Meredith, and R. R. Anderson (2005), Timescale for radiation belt electron acceleration by whistler mode chorus waves, *Journal of Geophysical Research: Space Physics*, *110* (A3), n/a–n/a, doi:10.1029/2004JA010811.

Horne, R. B., S. A. Glauert, R. M. Thorne (2003), Resonant diffusion of radiation belt electrons by whistler-mode chorus, *Geophysical Research Letters*, *30* (9), n/a–n/a, doi:10.1029/2003GL016963.

Horne, R. B., and R. M. Thorne (2003), Relativistic electron acceleration and precipitation during resonant interactions with whistler-mode chorus, *Geophysical Research Letters*, *30* (10), n/a–n/a, doi:10.1029/2003GL016973, 1527.

Keika, K., M. Nosé, S. Ohtani, K. Takahashi, S. P. Christon, and R. W. McEntire (2005), Outflow of energetic ions from the magnetosphere and its contribution to the decay of the storm time ring current, *Journal of Geophysical Research: Space Physics*, *110* (A9), n/a–n/a, doi:10.1029/2004JA010970, a09210.

Kennel, C. F., and H. E. Petschek (1966), Limit on stably trapped particle fluxes, *Journal of Geophysical Research*, *71* (1), 1–28, doi:10.1029/JZ071i001p00001.

Kilpua, E. K. J., H. Hietala, D. L. Turner, H. E. J. Koskinen, T. I. Pulkkinen, J. V. Rodriguez, G. D. Reeves, S. G. Claudepierre and H. E. Spence (2015), Unraveling the drivers of the storm time radiation belt response, *Geophysical Research*

Letters,*42*(9),3076–3084,doi:10.1002/2015GL063542.

Kletzing, C., W. Kurth, M. Acuna, R. MacDowall, R. Torbert, T. Averkamp, D. Bodet, S. Bounds, M. Chutter, J. Connerney, D. Crawford, J. Dolan, R. Dvorsky, G. Hospodarsky, J. Howard, V. Jordanova, R. Johnson, D. Kirchner, B. Mokrzycki, G. Needell, J. Odom, D. Mark, J. Pfaff, R., J. Phillips, C. Piker, S. Remington, D. Rowland, O. Santolik, R. Schnurr, D. Sheppard, C. Smith, R. Thorne, and J. Tyler (2013), The electric and magnetic field instrument suite and integrated science (emfisis) on rbsp, *Space Science Reviews*,*179*(1-4),127–181, doi:10.1007/s11214-013-9993-6.

Lakhina, G. S., B. T. Tsurutani, O. P. Verkhoglyadova, and J. S. Pickett (2010), Pitch angle transport of electrons due to cyclotron interactions with the coherent chorus subelements, *Journal of Geophysical Research: Space Physics*, *115*(A8), n/a–n/a, doi:10.1029/2009JA014885, a00F15.

Lam, M. M., R. B. Horne, N. P. Meredith, S. A. Glauert, T. Moffat-Griffin, and J. C. Green (2010), Origin of energetic electron precipitation ¿30 kev into the atmosphere, *Journal of Geophysical Research: Space Physics*, *115*(A4), n/a–n/a, doi:10.1029/2009JA014619, a00F08.

Li, W., Y. Y. Shprits, and R. M. Thorne (2007), Dynamic evolution of energetic outer zone electrons due to wave-particle interactions during storms, *Journal of Geophysical Research: Space Physics*, *112*(A10220), n/a–n/a, doi:10.1029/2007JA012368.

Loto'aniu, T. M., H. J. Singer, C. L. Waters, V. Angelopoulos, I. R. Mann, S. R. Elkington, and J. W. Bonnell (2010), Relativistic electron loss due to ultralow frequency waves and enhanced outward radial diffusion, *Journal of Geophysical Research: Space Physics*, *115*(A12), n/a–n/a, doi:10.1029/2010JA015755.

Lyons, L. R., and R. M. Thorne (1972), Parasitic pitch angle diffusion of radiation belt particles by ion cyclotron waves, *Journal of Geophysical Research*, *77*(28), 5608–5616, doi:10.1029/JA077i028p05608.

Matsumura, C., Y. Miyoshi, K. Seki, S. Saito, V. Angelopoulos, and J. Koller (2011), Outer radiation belt boundary location relative to the magnetopause: Implications for magnetopause shadowing, *Journal of Geophysical Research: Space Physics*, *116*(A6), n/a–n/a, doi:10.1029/2011JA016575, a06212.

McComas, D., S. Bame, P. Barker, W. Feldman, J. Phillips, P. Riley, and J. Griffee (1998), Solar wind electron proton alpha monitor (swepam) for the advanced composition explorer, *Space Science Reviews*, *86*(1–4), 563–612, doi:10.1023/A:1005040232597.

Miyoshi, Y., and R. Kataoka (2005), Ring current ions and radiation belt electrons during geomagnetic storms driven by coronal mass ejections and corotating interaction regions, *Geophysical Research Letters*, *32*(21), n/a–n/a, doi:10.1029/2005GL024590, l21105.

Morley, S. K., R. H. W. Friedel, T. E. Cayton, and E. Noveroske (2010a), A rapid, global and prolonged electron radiation belt dropout observed with the global positioning system constellation, *Geophysical Research Letters*, *37*(6), n/a–n/a, doi: 10.1029/2010GL042772, l06102.

Morley, S. K., R. H. W. Friedel, E. L. Spanswick, G. D. Reeves, J. T. Steinberg, J. Koller, T. Cayton, and E. Noveroske (2010b), Dropouts of the outer electron radiation belt in response to solar wind stream interfaces: global positioning system observations, *Proceedings of the Royal Society of London A: Mathematical, Physical and Engineering*

Sciences, *466*(2123), 3329–3350.

Omura, Y., Y. Katoh, and D. Summers (2008), Theory and simulation of the generation of whistler-mode chorus, *Journal of Geophysical Research: Space Physics*, *113*(A4), n/a–n/a, doi:10.1029/2007JA012622, a04223.

Paschmann, G., and P. W. Daly (1998), Analysis Methods for Multi-Spacecraft Data. ISSI Scientific Reports Series SR-001, ESA/ISSI, Vol. 1. ISBN 1608-280X, 1998, *ISSI Scientific Reports Series*, *1*.

Reeves, G. D., K. L. McAdams, R. H. W. Friedel, and T. P. O'Brien (2003), Acceleration and loss of relativistic electrons during geomagnetic storms, *Geophysical Research Letters*, *30*(10), n/a–n/a, doi:10.1029/2002GL016513,1529.

Reeves, G. D., H. E. Spence, M. G. Henderson, S. K. Morley, R. H. W. Friedel, H. O. Funsten, D. N. Baker, S. G. Kanekal, J. B. Blake, J. F. Fennell, S. G. Claudepierre, R. M. Thorne, D. L. Turner, C. A. Kletzing, W. S. Kurth, B. A. Larsen, and J. T. Niehof (2013), Electron acceleration in the heart of the van allen radiation belts, *Science*, *341*(6149), 991–994, doi:10.1126/science.1237743.

Roederer, J. G.(1970), Dynamics of geomagnetically trapped radiation, in *Physics and Chemistry in Space*, ed. by J. G. Roederer, J. Zahringer, vol. 2 (Springer, Berlin, 1970).

Santolík, O., C. A. Kletzing, W. S. Kurth, G. B. Hospodarsky, and S. R. Bounds (2014), Fine structure of large-amplitude chorus wave packets, *Geophysical Research Letters*, *41*(2), 293–299, doi:10.1002/2013GL058889, 2013GL058889.

Shprits, Y. Y., R. M. Thorne, R. Friedel, G. D. Reeves, J. Fennell, D. N. Baker, and S. G. Kanekal (2006), Outward radial diffusion driven by losses at magnetopause, *Journal of*

Geophysical Research: Space Physics, *111*(A11), n/a–n/a, doi:10.1029/2006JA011657.

Shprits, Y. Y., N. P. Meredith, and R. M. Thorne (2007), Parameterization of radiation belt electron loss timescales due to interactions with chorus waves, *Geophysical Research Letters*, *34*(11), n/a–n/a, doi:10.1029/2006GL029050, l11110.

Shprits, Y. Y., D. A. Subbotin, N. P. Meredith, and S. R. Elkington (2008), Review of modeling of losses and sources of relativistic electrons in the outer radiation belt ii: Local acceleration and loss, *Journal of Atmospheric and Solar-Terrestrial Physics*, *70*(14), 1694–1713, doi:http://dx.doi.org/10.1016/j.jastp.2008.06.014, dynamic Variability of Earth's Radiation BeltsAGU Fall Meeting.

Smith, C., J. L'Heureux, N. Ness, M. Acuña, L. Burlaga, and J. Scheifele (1998), The ace magnetic fields experiment, *Space Science Reviews*, *86*(1–4), 613–632, doi:10.1023/A:1005092216668.

Su, Z., F. Xiao, H. Zheng, and S. Wang (2010), Combined radial diffusion and adiabatic transport of radiation belt electrons with arbitrary pitch angles, *Journal of Geophysical Research: Space Physics*, *115*(A10), n/a–n/a, doi:10.1029/2010JA015903, a10249.

Su, Z., F. Xiao, H. Zheng, and S. Wang (2011a), Radiation belt electron dynamics driven by adiabatic transport, radial diffusion, and wave-particle interactions, *Journal of Geophysical Research: Space Physics*, *116*(A4), n/a–n/a, doi:10.1029/2010JA016228, a04205.

Su, Z., F. Xiao, H. Zheng, and S. Wang (2011b), CRRES observation and STEERB simulation of the 9 October 1990 electron radiation belt dropout event, *Geophysical Research Letters*, *38*(L06), n/a–n/a, doi:10.1029/2011GL046873.

Su, Z., H. Zhu, F. Xiao, H. Zheng, C. Shen, Y. Wang and S. Wang (2012), Bounce-averaged advection and diffusion coefficients for monochromatic electromagnetic ion cyclotron wave: Comparison between test-particle and quasi-linear models, *Journal of Geophysical Research: Space Physics*, *117*(A9), n/a–n/a, doi:10.1029/2012JA017917, A09222.

Su, Z., F. Xiao, H. Zheng, Z. He, H. Zhu, M. Zhang, C. Shen, Y. Wang, S. Wang, C. A. Kletzing, W. S. Kurth, G. B. Hospodarsky, H. E. Spence, G. D. Reeves, H. O. Funsten, J. B. Blake, D. N. Baker (2014), Nonstorm time dynamics of electron radiation belts observed by the Van Allen Probes, *Geophysical Research Letters*, *41*(2), 229–235, doi:10.1002/2013GL058912.

Summers, D., C. Ma, and T. Mukai (2004), Competition between acceleration and loss mechanism of relativistic electrons during geomagnetic storms, *Journal of Geophysical Research: Space Physics*, *109*(A04221), n/a–n/a, doi:10.1029/2004JA010437.

Summers, D., B. Ni, and N. P. Meredith (2007), Timescales for radiation belt electron acceleration and loss due to resonant wave-particle interactions: 2. Evaluation for VLF chorus, ELF hiss, and electromagnetic ion cyclotron waves, *Journal of Geophysical Research: Space Physics*, *112*(A04207), n/a–n/a, doi:10.1029/2006JA011993.

Thorne, R. M., T. P. OBrien, Y. Y. Shprits, D. Summers, and R. B. Horne (2005), Timescales for MeV electron microburst loss during geomagnetic storm, *Journal of Geophysical Research: Space Physics*, *110*(A9), n/a–n/a, doi:10.1029/2004JA010882, A09202.

Thorne, R. M., W. Li, B. Ni, Q. Ma, J. Bortnik, L. Chen, D. N. Baker, H. E. Spence, G. D. Reeves M. G. Henderson, C. A. Kletzing, W. S. Kurth, G. B. Hospodarsky, J. B. Blake, J. F. Fenell, S. G. Claudepierre, and S. G. Kanekal (2013), Rapid local acceleration of relativistic radiation belt electrons by magnetospheric chorus, *Nature*, *504*(7480), 411–414,doi:10.1038/nature12889.

Thorne, R. M. (2010), Radiation belt dynamics: The importance of wave-particle interactions, *Geophysical Research Letters*, *37*(22), n/a–n/a, doi:10.1029/2010GL044990, l22107.

Thorne, R. M., and C. F. Kennel (1971), Relativistic electron precipitation during magnetic storm main phase, *Journal of Geophysical Research*, *76*(19), 4446–4453, doi:10.1029/JA076i019p04446.

Tóth, G., B. van der Holst, I. V. Sokolov, D. L. D. Zeeuw, T. I. Gombosi, F. Fang, W. B. Manchester, X. Meng, D. Najib, K. G. Powell, Q. F. Stout, A. Glocer, Y.-J. Ma, and M. Opher (2011), Adaptive numerical algorithms in space weather modeling, *Journal of Computational Physics*, *231*(3), 870 – 903, doi:http://dx.doi.org/10.1016/j.jcp.2011.02.006.

Tsurutani, B. T., and W. D. Gonzalez (1995), The efficiency of "viscous interaction" between the solar wind and the magnetosphere during intense northward imf events, *Geophysical Research Letters*, *22*(6), 663–666, doi:10.1029/95GL00205.

Tsurutani, B. T., and G. S. Lakhina (1997), Some basic concepts of wave-particle interactions in collisionless plasmas, *Reviews of Geophysics*, *35*(4), 491–501, doi:10.1029/97RG02200.

Tsurutani, B. T., and E. J. Smith (1974), Postmidnight chorus: A substorm phenomenon, *Journal of Geophysical Research*, *79*(1), 118–127, doi:10.1029/JA079i001p00118.

Tsurutani, B. T., and E. J. Smith (1977), Two types of magnetospheric elf chorus and their substorm dependences, *Journal of Geophysical Research*, *82*(32), 5112–5128, doi:10.1029/JA082i032p05112.

Tsurutani, B. T., O. P. Verkhoglyadova, G. S. Lakhina, and S. Yagitani (2009), Properties of dayside outer zone chorus during hildcaa events: Loss of energetic electrons, *Journal of Geophysical Research: Space Physics*, *114*(A3), n/a–n/a, doi:10.1029/2008JA013353, a03207.

Tsurutani, B. T., G. S. Lakhina, and O. P. Verkhoglyadova (2013), Energetic electron ($>$ 10 kev) microburst precipitation, $\sim$ 5–15 s x-ray pulsations, chorus, and wave-particle interactions: A review, *Journal of Geophysical Research: Space Physics*, *118*(5), 2296–2312, doi:10.1002/jgra.50264.

Turner, D. L., V. Angelopoulos, W. Li, M. D. Hartinger, M. Usanova, I. R. Mann, J. Bortnik, and Y. Shprits (2013), On the storm-time evolution of relativistic electron phase space density in earth's outer radiation belt, *Journal of Geophysical Research: Space Physics*, *118*(5), 2196–2212, doi:10.1002/jgra.50151.

Turner, D. L., V. Angelopoulos, W. Li, J. Bortnik, B. Ni, Q. Ma, R. M. Thorne, S. K. Morley, M. G. Henderson, G. D. Reeves, M. Usanova, I. R. Mann, S. G. Claudepierre, J. B. Blake, D. N. Baker, C.-L. Huang, H. Spence, W. Kurth, C. Kletzing, and J. V. Rodriguez (2014a), Competing source and loss mechanisms due to wave-particle interactions in earth's outer radiation belt during the 30 september to 3 october 2012 geomagnetic storm, *Journal of Geophysical Research: Space Physics*, *119*(3), 1960–1979, doi:10.1002/2014JA019770, 2014JA019770.

Turner, D. L., V. Angelopoulos, S. K. Morley, M. G. Henderson, G. D. Reeves, W. Li, D. N. Baker,C.-L. Huang, A. Boyd, H. Spence, S. G. Claudepierre, J. B. Blake and J. V. Rodriguez (2014b), On the cause and extent of outer radiation belt losses during the 30 September 2012 dropout event, *Journal of Geophysical Research: Space Physics*, *119*(3), 1530–1540, doi:10.1002/2013JA019446, 2013JA019446.

Ukhorskiy, A. Y., Y. Y. Shprits, B. J. Anderson, K. Takahashi, and R. M. Thorne (2010), Rapid scattering of radiation belt electrons by storm-time emic waves, *Geophysical Research Letters*, *37*(9), n/a–n/a, doi:10.1029/2010GL042906, l09101.

Table 1. Parameters used in equation 1 for the 21:25 – 22:00 UT interval on September 12, 2014.

Chorus Subelement	Initial Time (UT)	τ (ms)	T (ms)	B_{max} (nT)	B_o (nT)	$2\pi f/\Omega$	Δt_τ (ms)	Δt_T (ms)	$\Delta\alpha_\tau$ (°)	$\Delta\alpha_T$ (°)
1	21:29:05.233	13	3.0	0.80	78	0.155	2.80	0.64	4.59	1.06
2	21:29:05.362	14	3.0	0.76	78	0.155	3.00	0.65	4.70	1.00
3	21:29:05.959	14	3.5	0.76	78	0.155	3.00	0.75	4.70	1.18
4	21:29:06.584	11	3.5	0.97	79	0.153	2.30	0.75	4.66	1.48
5	21:46:56.248	13	3.5	0.63	69	0.145	2.60	0.71	3.42	0.92
6	21:52:55.444	13	3.0	0.88	65	0.185	2.30	0.76	5.94	1.37
7	21:52:55.906	11	2.5	1.16	65	0.185	2.80	0.63	6.62	1.50
8	21:52:56.524	14	2.5	0.92	65	0.185	3.50	0.63	6.68	1.19
9	21:52:58.480	22	3.0	0.90	65	0.185	5.60	0.76	10.28	1.40
10	21:52:59.071	9	2.5	0.65	65	0.185	2.30	0.63	3.03	0.84
11	21:52:59.332	11	3.0	0.86	65	0.185	2.80	0.76	4.90	1.34

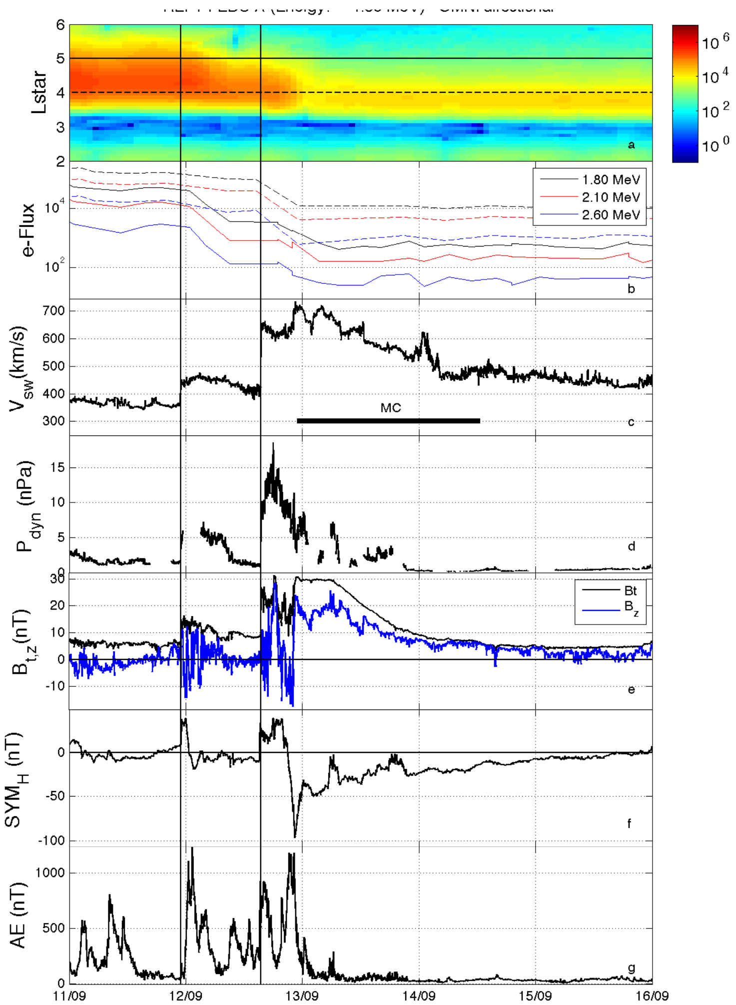

Figure 1. Relativistic electron flux in the outer radiation belt, solar wind parameters and geomagnetic indexes observed from September 11 – 16, 2014. (a) Electron flux in the 1.8 MeV energy channel measured by REPT on board Van Allen Probe A as a function of time and L^*; (b) electron flux measured for three energy channels at $L^* \sim 4$ (dashed lines) and $L^* \sim 5$ (solid lines) as a function of time; (c) solar wind speed, and the solid bar indicating the magnetic cloud (MC) period; (d) dynamic pressure; (e) IMF strength (B_t, black line) and north-south component (B_z, blue line); (f) symmetric disturbance time index Sym-H and (g) auroral electrojet AE index. The two vertical line indicate the first and second shock arrival times, 23:50 UT on September 11 and 16:00 UT on September 12, respectively.

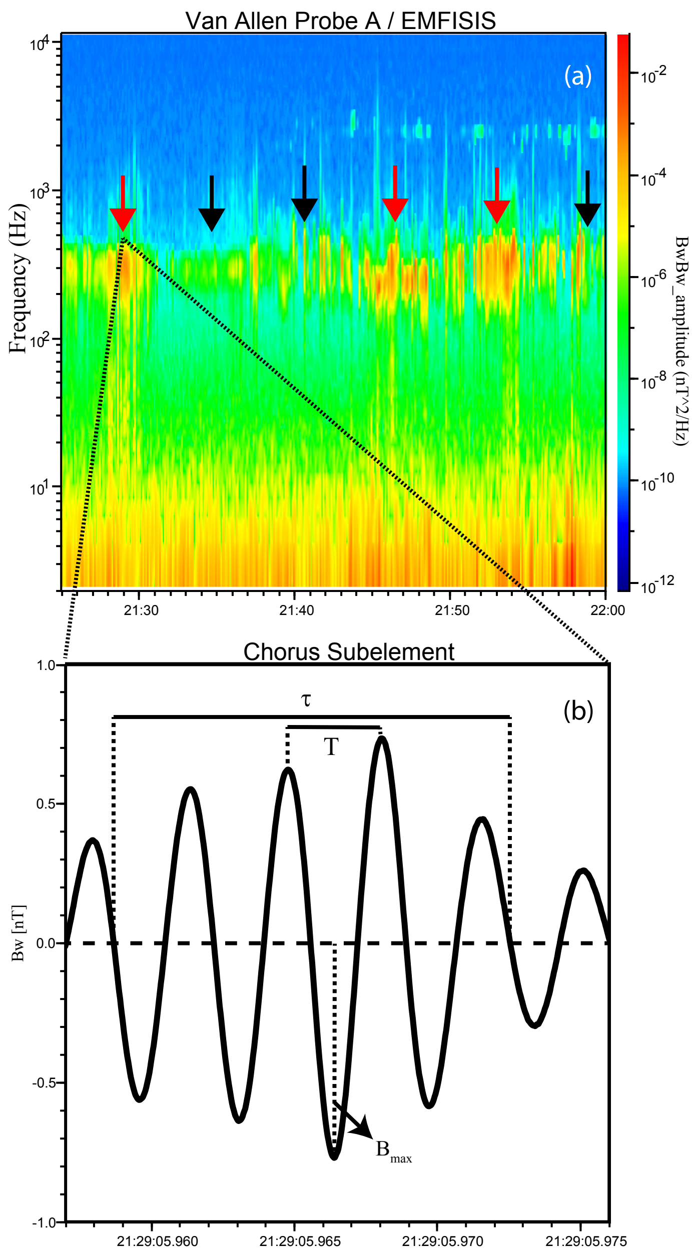

Figure 2. (a) EMFISIS' magnetic field spectrogram measured at $L^* \sim 5$ and MLAT $\sim 2^\circ$ for a 35 minutes period within the storm's main phase on late September 12. The electron cut-off gyrofrequency divided by two varied between 5.2 and 7.4 kHz, and the corresponding mean value was 6.3 kHz. Arrows indicate when burst mode data was available for the selected period. Red arrows indicate periods when a selected chorus subelement (panel b) had a wave magnetic field amplitude $B_w \gtrsim 0.5nT$. Panel (b) shows high resolution magnetic field measurements corresponding to a period of higher magnetic spectral density. Several chorus subelements were identified in this dataset and panel (b) shows an example of it. Relevant parameters used in equation (1) are identified as: B_{max}, the maximum instantaneous absolute value of the wave amplitude, T corresponding to one wave-cycle period, and τ the subelement's time duration.

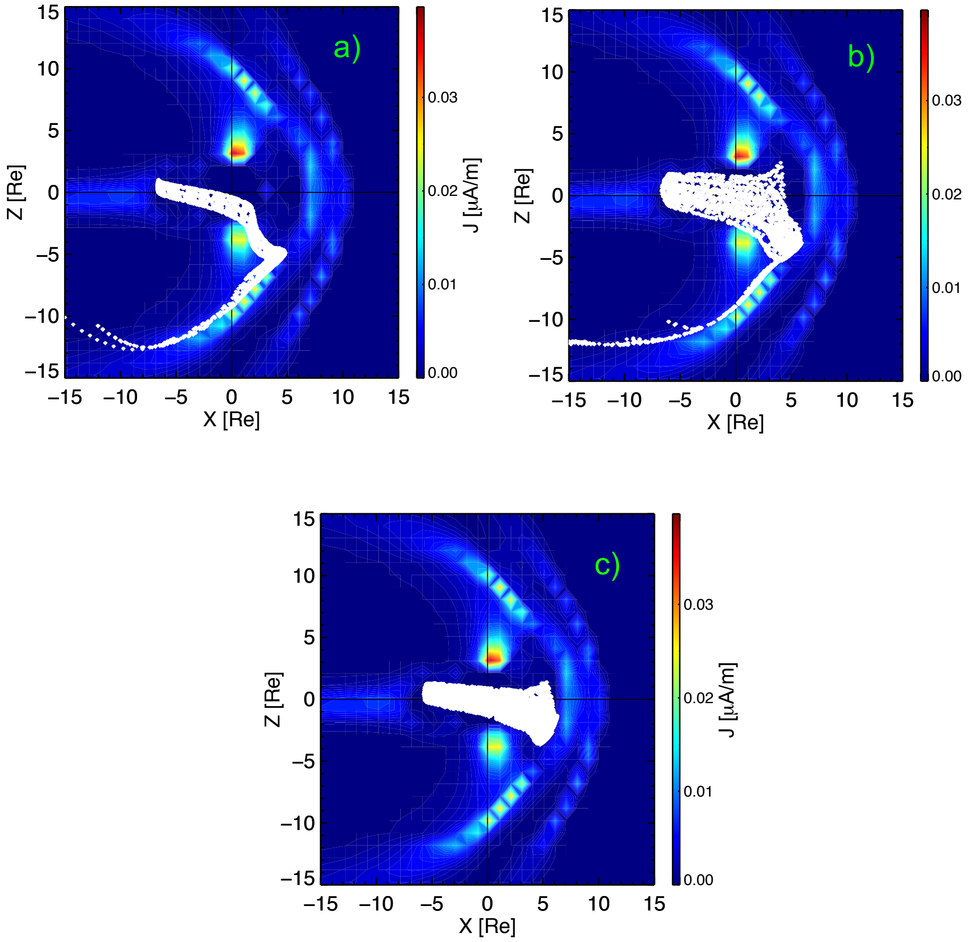

Figure 3. Electron's drift orbit calculation during the time when the magnetosphere was most compressed due to the arrival of the second interplanetary shock. The time-stationary magnetic field used in the orbit's calculation was simulated by the 3D MHD BATS-R-US code. The color contour represent the magnetospheric current density as simulated by BATS-R-US. The orbits showed are representative for the following starting positions (a) $-8 \leq$ X $\leq$ -6.6 R_E, (b) -6.6 $<$ X $\leq$ -5.5 R_E, and (c) X $>$ -5.5 R_E. All orbits starts at the equatorial plane, i.e., (Y,Z) = (0,0).